

# Dalton Transactions

Accepted Manuscript



This is an *Accepted Manuscript*, which has been through the Royal Society of Chemistry peer review process and has been accepted for publication.

*Accepted Manuscripts* are published online shortly after acceptance, before technical editing, formatting and proof reading. Using this free service, authors can make their results available to the community, in citable form, before we publish the edited article. We will replace this *Accepted Manuscript* with the edited and formatted *Advance Article* as soon as it is available.

You can find more information about *Accepted Manuscripts* in the [Information for Authors](#).

Please note that technical editing may introduce minor changes to the text and/or graphics, which may alter content. The journal's standard [Terms & Conditions](#) and the [Ethical guidelines](#) still apply. In no event shall the Royal Society of Chemistry be held responsible for any errors or omissions in this *Accepted Manuscript* or any consequences arising from the use of any information it contains.

# A Little Spin on the Side: Solvent and Temperature Dependent Paramagnetism in $[\text{Ru}^{\text{II}}(\text{bpy})_2(\text{phendione})]^{2+}$

Robert D. Schmidt, Caleb A. Kent, Javier J. Concepcion,  
Wenbin Lin, Thomas J. Meyer, and Malcolm D. E. Forbes\*

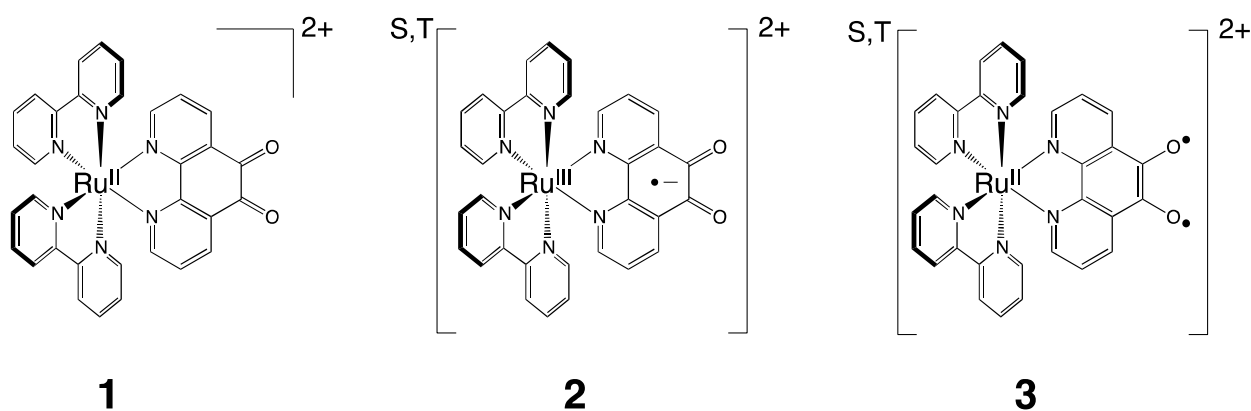
*Caudill and Murray Laboratories*  
*Department of Chemistry, CB #3290*  
*University of North Carolina at Chapel Hill*  
*Chapel Hill, NC, 27599-3290*  
[\\*mdef@unc.edu](mailto:mdef@unc.edu)

**Abstract:** Solvent and temperature dependent paramagnetism is reported for the complex  $[\text{Ru}^{\text{II}}(\text{bpy})_2(\text{phendione})](\text{PF}_6)_2$  (bpy = 2,2'-bipyridine, phendione = 1,10-phenanthroline-5,6-dione), **1**. Magnetometry,  $^1\text{H-NMR}$ , EPR and substituent effects confirm that the paramagnetic character is localized on the phendione ligand, and arises due to mixing of the MLCT excited state with an open shell triplet state on the phendione moiety, a process that is most likely driven by aromatization. The stabilized open shell phendione structure, in which the triplet lies lower in energy than the singlet, can then be thermally populated from the ground state of the complex. This process is facilitated by admixture of singlet character from the MLCT state. Paramagnetic behavior is absent in the free phendione ligand, and disappears in the presence of Lewis acids and in the presence of water due to hydrogen bonding (or hydrate formation at sufficient water concentrations). Control experiments rule out the presence of monoradicals such as semiquinone anions. Implications for spin filtering, sensing, and other electronic applications using such structures are discussed.

## Introduction

Electronic interactions between metal centers and open-shell organic structures present intriguing opportunities for applications in spintronics<sup>1</sup> and sensing<sup>2</sup>, and challenges for computational chemists seeking to understand the balance of magnetic and redox properties in such species.<sup>3</sup> A key feature of many of these applications is the ability to control molecular magnetic behavior as needed through external stimuli. In this paper we report a novel example of such control arising from a coordination-dependent contribution from an open-shell biradicaloid form of the phendione ligand in the complex  $[\text{Ru}^{\text{II}}(\text{bpy})_2(\text{phendione})](\text{PF}_6)_2$  (**1**):

### Chart 1



The contribution of open shell configurations (Chart 1) to the structure of **1** is most likely facilitated by configuration interaction involving higher metal to ligand charge transfer (MLCT) excited states, of which structure **2** above is drawn as a general example (there are multiple ligand anion sites, and each MLCT state can have a singlet (S) or triplet (T) spin configuration). Since the MLCT triplet state is expected to lie below its corresponding singlet state in energy, it will mix with the ligand triplet state **3**, lowering its energy and thereby providing a thermally accessible pathway to paramagnetic behavior in the parent compound. The thermal population

process is formally spin forbidden, but this restriction is lifted by admixture of singlet character in the MLCT state (see below for details).

While coordinated ligands modified by stable open-shell *monoradical* structures are known and well understood<sup>4</sup>, and stable biradicaloids from purely organic structures with extended conjugation have also been reported<sup>5-9</sup>, complex **1** offers a very unusual case of an open shell, two-electron spin system that is observable only upon metal coordination, and one that does not require significant extension of conjugation. In the open-shell (**3**) form, the phendione ring system aromatizes, offering some degree of stabilization, but the singlet-triplet (S-T) gap expected for the free ligand may still be large.<sup>10</sup> The presence of the Ru metal center, however, offers a dense excited state manifold (including state **2** which contains a Ru(III) coordination site), through which spin-orbit coupling and configuration interaction can stabilize the phendione ligand open shell singlet and/or triplet (**3**). Below we present structural and spectroscopic evidence for thermal population of the open shell triplet ligand state **3**, made possible by configuration interaction with MLCT state **2**. This phenomenon has not been reported previously for any coordination compound. Such a system provides a window of opportunity to test the stability and tunability of **1** and its derivatives for possible spin filtering applications<sup>11</sup> or the construction of novel sensors.<sup>2</sup>

## Results and Discussion

*A. Magnetic Resonance Measurements.* Temperature dependent <sup>1</sup>H NMR and EPR spectra of compound **1**, shown in Figure 1, confirm that a paramagnetic species is observable in solution near room temperature and the paramagnetic behavior appears to increase with increasing temperature. The line broadening in the <sup>1</sup>H NMR spectra and the corresponding increase in the

EPR signal intensity are reversible, i.e., the process can be cycled through many times with no loss of EPR signal or change in the broadening parameter in the NMR spectra. The complex was purified through vapor diffusion recrystallization of ether into MeCN prior to the experiments, and no degradation of the sample was ever observed.

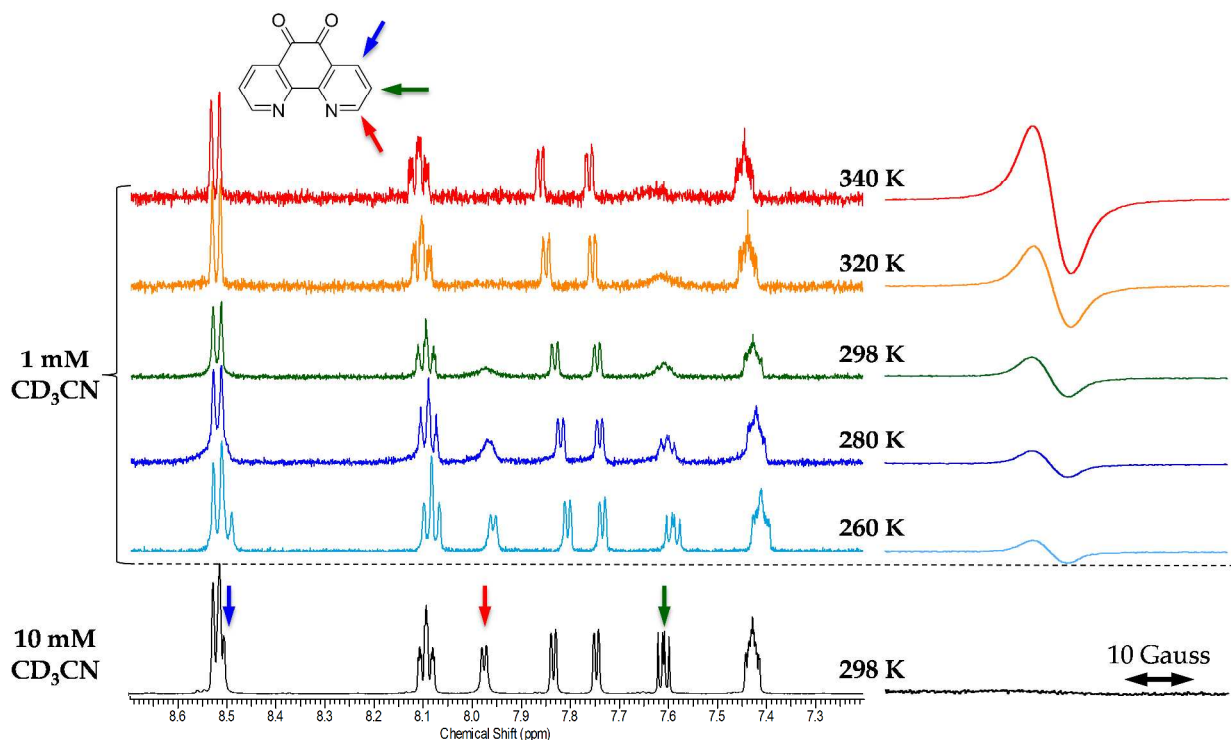


**Figure 1.** Top left: Variable temperature <sup>1</sup>H NMR spectra for a 1 mM sample of **1** in *d*<sup>3</sup>-acetonitrile collected from 260 K to 340 K. Bottom left: 10 mM sample at 298 K shown for reference. Color coded arrows indicate specific phendione protons. All NMR spectra are referenced to CD<sub>2</sub>HCN. Right: Variable temperature EPR spectra for **1** at 1 mM and 10 mM under identical conditions.

At 10 mM in dry *d*<sup>3</sup>-acetonitrile at room temperature, the <sup>1</sup>H-NMR spectrum obtained for **1** is the expected diamagnetic pattern (Figure 1, bottom left). Dilution of this sample to 1 mM shows broadening of specific features (see 298 K spectrum), a phenomenon which varied in magnitude over the temperature range 260 K to 340 K (Figure 1, left side). At temperatures below ca. 290 K, the (color-coded) phendione NMR resonances are sharp, showing the expected diamagnetic NMR spectrum. Above room temperature, the phendione resonances almost completely

disappear. There are also small downfield shifts of all the bipyridine (bpy) proton resonances with increasing temperature. The magnitude of each bpy proton shift depends on the proximity of the particular proton to the phendione ring. Broadening of selected lines as a function of proximity strongly suggests that the observed phenomenon is an intrinsic feature of the molecular structure of **1**, rather than an impurity which would be expected to affect every NMR transition equally.

It is noteworthy that the three phendione peaks begin to broaden at different rates with increasing temperature, and these rates should scale with the magnitude of the spin density at each position in the open shell triplet state **3**. Supporting Information Figure S1 shows the result of a density functional theory (DFT) calculation aimed at extracting the spin densities (Table S1) for the lowest energy triplet state of geometry optimized structure **3**. It should be noted that the energies of such structures are notoriously difficult to obtain due to their open shell nature<sup>12</sup>, and because the transition metal center has a large spin-orbit coupling parameter.<sup>13</sup> However, this level of calculation is sufficient for qualitative spin density evaluation.

Figure S1 and Table S1 help to explain the following observations: 1) that there is a small spin density contribution from Ru to the ground state electronic structure of **3**, 2) that the phendione protons marked by red and blue arrows (Figure 1, top) are much more sensitive to paramagnetic broadening than those marked green, and 3) that the bpy protons are also affected, but in a minor way (small shifts and no broadening). A similar localized broadening effect in the NMR spectra of Kekulé organic systems has been attributed to thermal population of a triplet made accessible through open-shell ground states, or resonance contributions in the ground state.<sup>5-9</sup>

The temperature induced broadening and shifting of the <sup>1</sup>H NMR signals (Figure 1, left side) directly correlate with an increase in the steady-state X-band EPR signal (Figure 1, right side) of

the 1 mM solution of **1** over the same temperature range. The peak-to-peak width of the EPR signal remains unchanged with increasing temperature. We attribute this signal to access, by thermal population, of the open shell ligand triplet state **3**. The EPR spectrum is averaged significantly due to fast tumbling in liquid solution. Because of this averaging, half-field lines or dipolar interactions are not directly observable in the spectrum.<sup>14</sup> To completely average the electron dipole-dipole interaction (D) in a triplet state to zero, the rotational correlation time should be approximately 5 times faster than the inverse of the D value. The D value for the MLCT triplet state or the ligand triplet state should be comparable to a typical organic carbonyl triplet state, i.e, about  $0.1 \text{ cm}^{-1}$ , giving a frequency of  $3 \times 10^9 \text{ s}^{-1}$ , the inverse of which is  $3 \times 10^{-10} \text{ s}$ . To average the dipolar interaction to zero therefore requires a rotational correlation time 5 times shorter, or  $6 \times 10^{-11} \text{ s}$  (60 ps). It is highly unlikely that this complex could rotate at 60 ps even in the gas phase, so some remnant of the triplet state spectrum will remain in solution, and the exact width and line shape is difficult to predict.

*B. Magnetic Susceptibility.* Results of magnetometry measurements of **1** in the solid state confirm the paramagnetic character (Figure 2) of the complex. The  $\chi_{para} \cdot T$  vs. T data exhibit a straight line with a positive slope (Figure 2A), which is indicative of a large  $\chi_{TIP}$  component.<sup>15</sup> The value of  $\chi_{para} \cdot T$  tends to zero at low temperatures, supporting the hypothesis of a singlet ground state. It is higher than 1.0 because there is a deviation from  $g = 2.0$  due to the presence of the metal. A subtraction of the straight line whose slope was calculated from the plot in Figure 2A was carried out, in order to separate the temperature independent contribution to the value of  $\chi_{para} \cdot T$ . This process reveals significant curvature at higher temperatures, which is indicative of a contribution to the susceptibility from a thermally accessible paramagnetic state (Figure 2B). This result is corroborated by the very precise overlap of the normalized magnetometry curve

(red line in Figure 2B) with the temperature-dependent solid state EPR signal intensities (blue dots in Figure 2B, acquired by double integration of the EPR signals as a function of temperature; representative room temperature spectra for a solid state sample of **1** are shown in Figure 3.

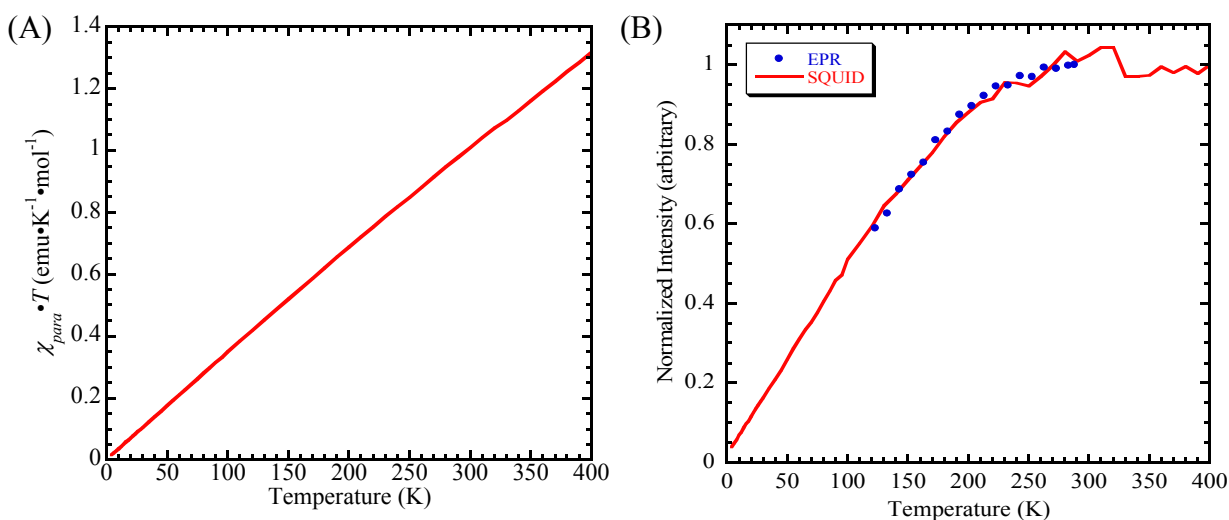


**Figure 2.** Magnetic susceptibility (SQUID measurements) plotted as  $\chi_{para} \cdot T$  vs.  $T$  for a solid (powder) sample of **1**. (A) Uncorrected  $\chi_{para} \cdot T$  values; the positive slope component suggests a large  $\chi_{TIP}$ ; (B) Normalized  $\chi_{para} \cdot T$  values following subtraction of the straight line from Figure 2A, plotted here with the normalized solid state (neat powder) EPR signal intensity (blue dots).

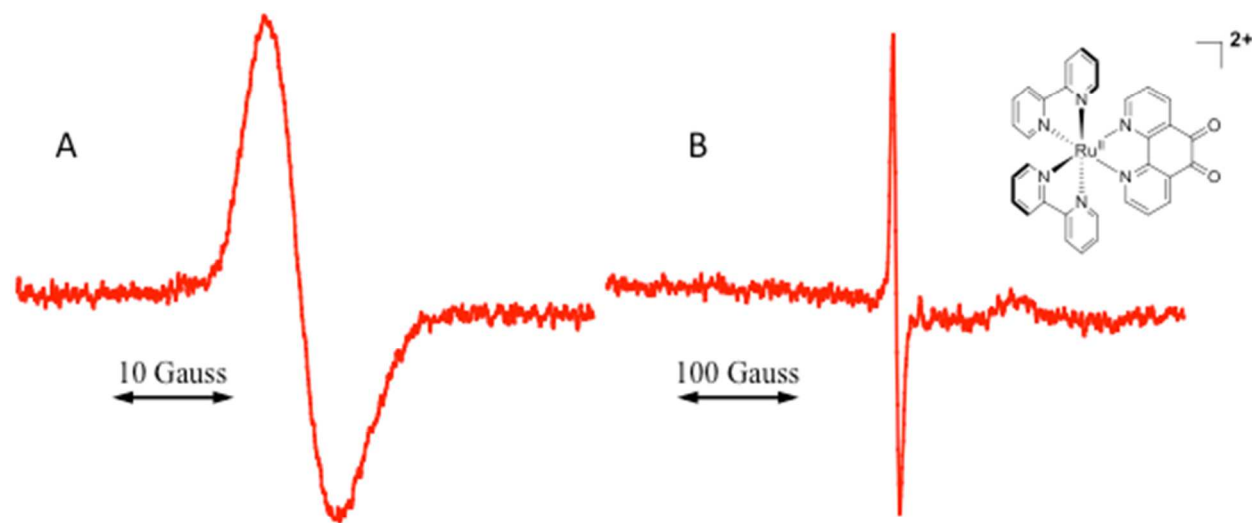


**Figure 3.** Room temperature (293 K) steady-state X-band EPR spectra for solid state (powder) samples of **1** collected at a center field of 3363.87 G, modulation amplitude of 5 G with (A) 50 G sweep width (B) 500 G sweep width. The small high field bump in B) is temperature independent and is unassigned. Double integration of spectra such as that in A) were used to provide the comparison shown in Figure 3B (blue dots) between the SQUID and EPR measurements as a function of temperature.

*C. Concentration Effects.* There is a pronounced concentration effect on the magnetic resonance spectra of complex **1**. For example, at the same temperature, a 10 mM solution of **1** shows a sharp  $^1\text{H}$  NMR spectrum (Figure 1 bottom), compared to the spectrum observed at 1 mM (Figure 1, left side, central (green) spectrum). Correspondingly, a weak EPR spectrum is observed for complex **1** at high concentrations ( $> 3$  mM), but the spectrum becomes *more intense* at higher dilutions until the spectrometer sensitivity is affected; thereafter the EPR signal decreases in intensity with decreasing concentration (Figure 4). This point is critical: a paramagnetic state with *one unpaired electron* (ruled out further by additional experiments, *vide infra*) would show a monotonic increase in signal intensity with concentration. At higher concentrations, one- or two-electron spin systems will undergo rapid spin lattice relaxation (concentration dependent Heisenberg spin exchange), but the two-electron system can also undergo triplet-triplet annihilation processes, leading to a decrease in signal intensity. Both mechanisms can be operative in solution EPR spectra of triplet states at these concentrations.<sup>16</sup> However, we note that only intensities, and not the line widths, are changing in Figure 4A. This indicates that Heisenberg spin exchange between paramagnetic sites cannot be responsible for the observed behavior.

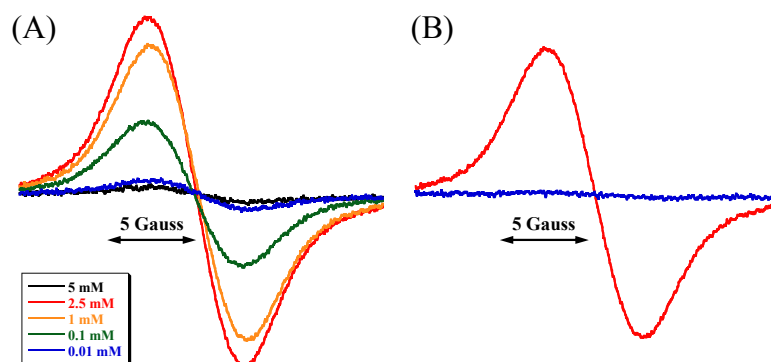


**Figure 4.** Initial EPR spectra of **1**: (A) Concentration dependence of the EPR signal intensity, (B) 1 mM CD<sub>3</sub>CN NMR Sample (red) vs. 1 mM CD<sub>3</sub>CN/0.25% D<sub>2</sub>O NMR sample (blue).

The solid state (neat powder) EPR spectra shown in Figures 3A and 3B show narrow signals because the triplet-triplet interactions are very strong in close contact and this will lead to significant and fast electron spin relaxation. The solid-state spectrum in Figure 3A also has a very anisotropic line shape, typical for powder pattern triplets in polycrystalline samples.<sup>17</sup>

*D. Solvent Effects.* Running the  $^1\text{H}$  NMR experiment in dimethyl sulfoxide- $d_6$  (DMSO) also showed broadening of the phendione protons, which remained even at higher concentrations (10 mM) (Figure 5).

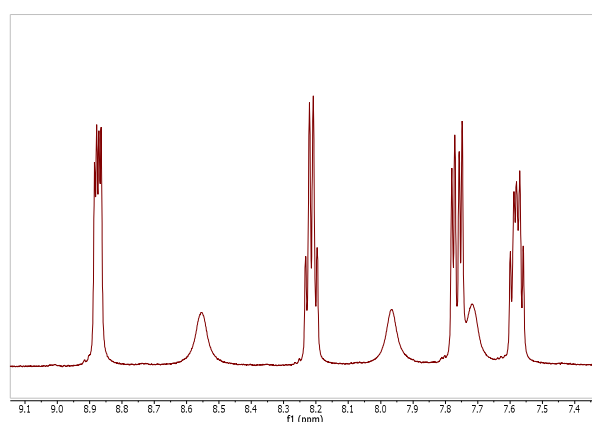


**Figure 5.**  $^1\text{H}$ -NMR spectrum of **1**, 10 mM in  $d_6$ -DMSO.

This solvent effect is most likely due to the increased viscosity of DMSO over MeCN (a factor of 5 more viscous than MeCN<sup>18</sup>), which will lead to an increase in the spin lattice relaxation time of the triplet (slower tumbling) and a decrease in the triplet-triplet annihilation rate due to decreased collisional frequencies. Addition of a Lewis acid (anhydrous  $\text{ZnCl}_2$ ) also sharpens the NMR spectrum (Figure 6), because of stabilization of the ground state phendione structure.

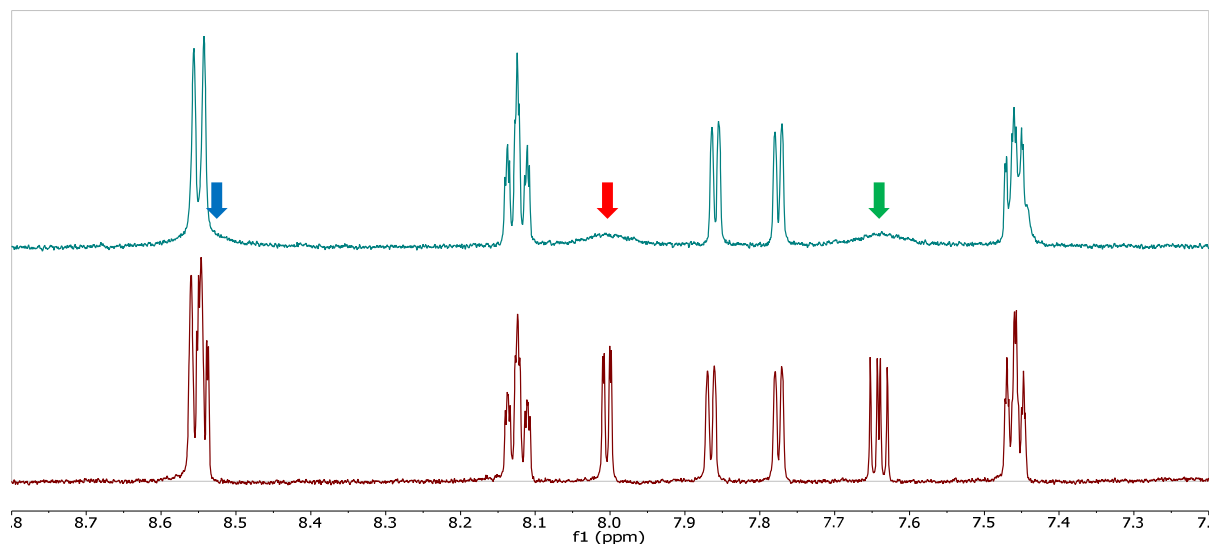
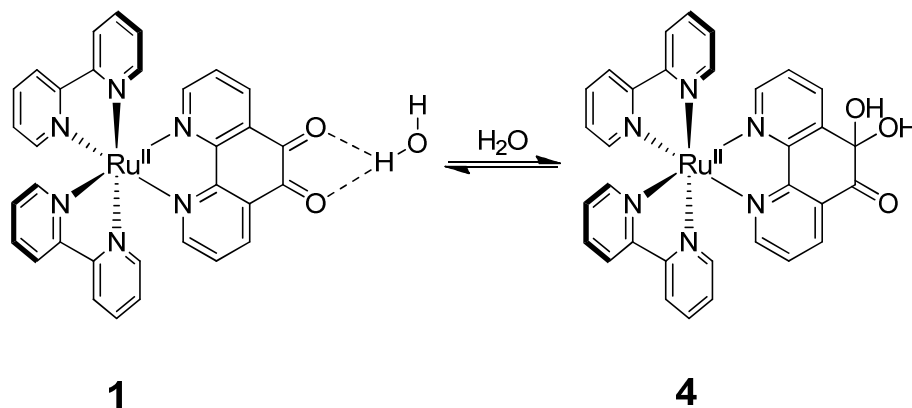


**Figure 6.**  $^1\text{H}$ -NMR spectra of aromatic region of **1** collected at 1 mM in  $\text{CD}_3\text{CN}$  (top) and with 50 mM anhydrous  $\text{ZnCl}_2$  in  $\text{CD}_3\text{CN}$  (bottom). The color coding of the arrows is the same as that in Figure 1 of the manuscript and represent the selected phendione ligand protons.

Addition of  $\text{D}_2\text{O}$  (0.25% by volume) to the 1 mM sample of **1** also produces a sharp NMR spectrum. If the NMR experiment is run in pure  $\text{D}_2\text{O}$  at 1 mM in **1**, the spectrum appears with significant signal shifts, new resonances, and broadening of some peaks (Supporting Information, Figure S2). The effect of water at low concentrations is attributed to hydrogen bonding, which stabilizes the ground state of the closed shell phendione structure **1**, reducing thermal accessibility to **3**. This is supported by the sharper NMR spectrum and a reduced EPR signal (e.g., Figure 4B) when water is added. In fact,  $\text{D}_2\text{O}$  virtually eliminates the EPR signal and  $\text{H}_2\text{O}$  reduces it by about half. The observed isotope effect correlates with that measured previously by Singh and Rao,<sup>19</sup> who found a  $K_{\text{H}}/K_{\text{D}}$  value of 0.7 for H-bonding of water in MeCN.

*E. Hydrate Formation.* The change in spectral features at very high water concentrations is most likely due to formation of the hydrate **4**, which is facilitated by coordination to the metal center, as the carbonyl carbons become activated toward nucleophilic substitution.<sup>20,21</sup> This is supported by optical emission experiments. Complex **1** is very weakly emissive in acetonitrile

solution (57  $\mu\text{M}$ ) with a  $\lambda_{\text{max}}$  of ca. 640 nm and a lifetime of 748 ns. With increasing water concentration, the emission gains intensity with a bathochromic shift, while the single exponential lifetime decreases (Figure 7).



Consistent with the energy gap law for nonradiative decay,<sup>22</sup> the decrease in lifetime is consistent with this bathochromic shift which increases vibrational overlap and the rate of non-radiative decay. Qualitatively, the increase in intensity is inconsistent with a shorter lifetime, since the quantum yield and lifetime are related by  $\phi = k_r/\tau$  with  $k_r$  the radiative decay rate constant. Reaction with water to form **4** breaks the quinoid core conjugation, lowering the electron accepting ability of the ligand. This eliminates dione quenching and MLCT emission appears.

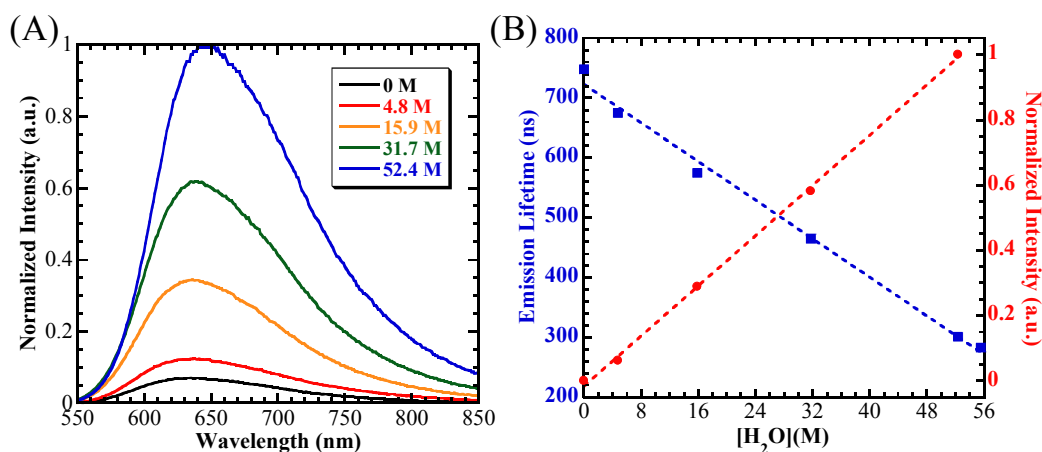


**Figure 7.** (A) Emission Spectra at the water concentrations indicated in the legend; (B) lifetime and intensity versus water concentration).

The hydration chemistry of phendione has been characterized previously by NMR and electrochemical methods, but is only observed with N-coordination to metals or a proton, activating the dione to nucleophilic attack.<sup>20,21,23</sup> The facile quenching observed for **1** is attributed to an intramolecular oxidative quenching mechanism,  $^3(d\pi^5\pi^*_{\text{bpy}})^1 \rightarrow ^3(d\pi^5\pi^*_{\text{dione}})^1$ , by the dione (an *o*-benzoquinone mimic), a quenching pathway that is not possible upon hydration and formation of **4**.

*F. Substituent Effects.* To understand electronic effects on the physical properties of **1** in more detail, several structural analogs were prepared with ligands more electron withdrawing (bis(diethyl [2,2'-bipyridine]-4,4'-dicarboxylate), deeb) and two that were more electron donating (bis(4,4'-dimethyl-2,2'-bipyridine), dmb) and bis(4,4',5,5'-tetramethyl-2,2'-bipyridine), tmb):

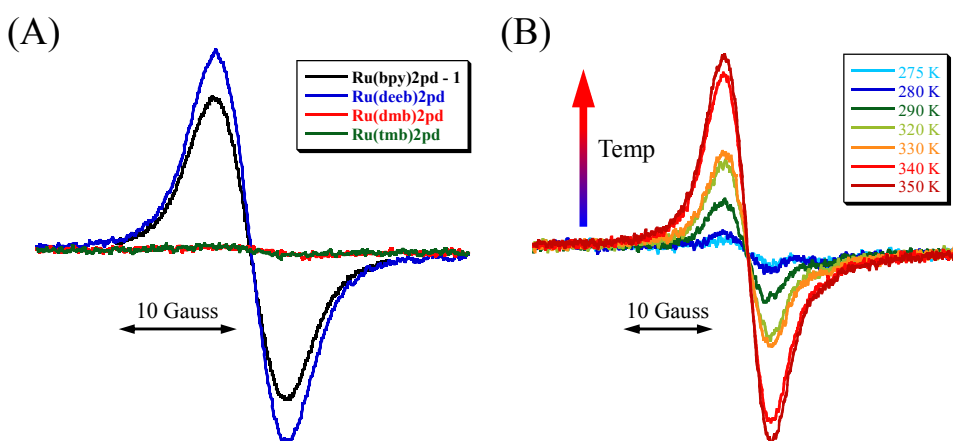
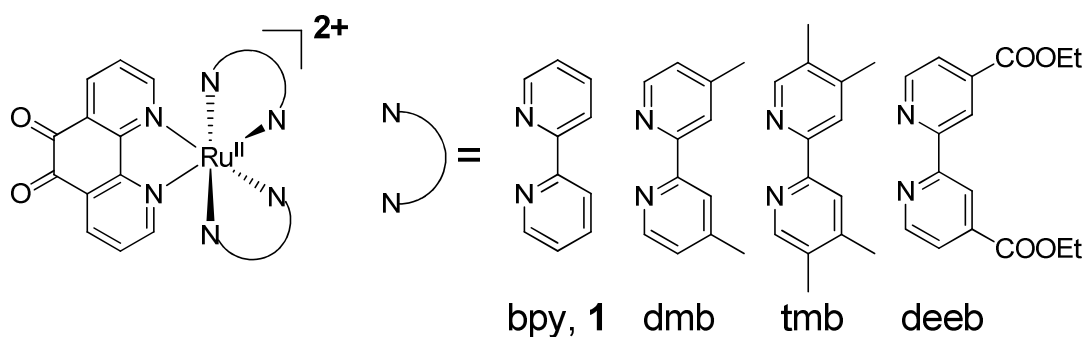


**Figure 8.** (A) EPR spectra of the indicated  $[\text{Ru}^{II}(\text{N-N})_2(\text{pd})]^{2+}$  complexes at 1mM concentration in MeCN at room temperature. (B) VT-EPR spectrum for  $[\text{Ru}^{II}(\text{deeb})_2\text{pd}]^{2+}$  at 1 mM in MeCN from 275-350 K.

Line broadening in the NMR spectra and intense EPR signals at 1 mM concentration were observed for the complex with the more electron-withdrawing deeb ligand, while the electron-donating dmb and tmb derivatives exhibited sharp NMR spectra under all conditions tested, and very weak EPR signals at 1 mM concentration (Figure 8A). Furthermore, the EPR spectral intensities from the deeb derivative showed strong temperature dependence (Figure 8B). The observed substituent effects are best understood in terms of the energy level diagram shown in Figure 10. Substituents on the bpy ring system have a large impact on the Ru(III/II) potential (a range of 360 mV) but only change the first phendione reduction potential by about 60 mV (Table 1).

Table 1. Experimental redox potentials and emission energies

N-N	Ru III/II (V vs Ag/Ag <sup>+</sup> )	pd/pd <sup>-</sup> (V vs Ag/Ag <sup>+</sup> )	Emission (nm)
tmb	0.948	-0.461	641
dmb	1.015	-0.453	642
bpy	1.110	-0.440	645
deeb	1.305	-0.400	647

These shifts, particularly on the Ru(III/II) potential, coupled with the spin density trends listed in Table 1, show that there is significantly more back-bonding to the bpy-substituents in the deeb complex than in the dmb/tmb complexes, which alters the degree of back-bonding to the phendione ligand. In the deeb complex, a more electron-deficient phendione ligand results, stabilizing the MLCT state(s) by stabilizing the ligand anion moiety. This leads to a large perturbation of state **3**, lowering its energy and increasing its thermal population from **1**.

The more electron-donating dmb/tmb complexes are less back-bonding and draw less electron density from the metal center, resulting in a more electron rich phendione. This condition favors the dione form, reducing the overall contribution of the biradicaloid state in the ground state

electronic structure, but more importantly destabilizing the MLCT state(s), consistent with the reduction in EPR signal intensity for the dmb/tmb complexes, as state **3** is now higher in energy.

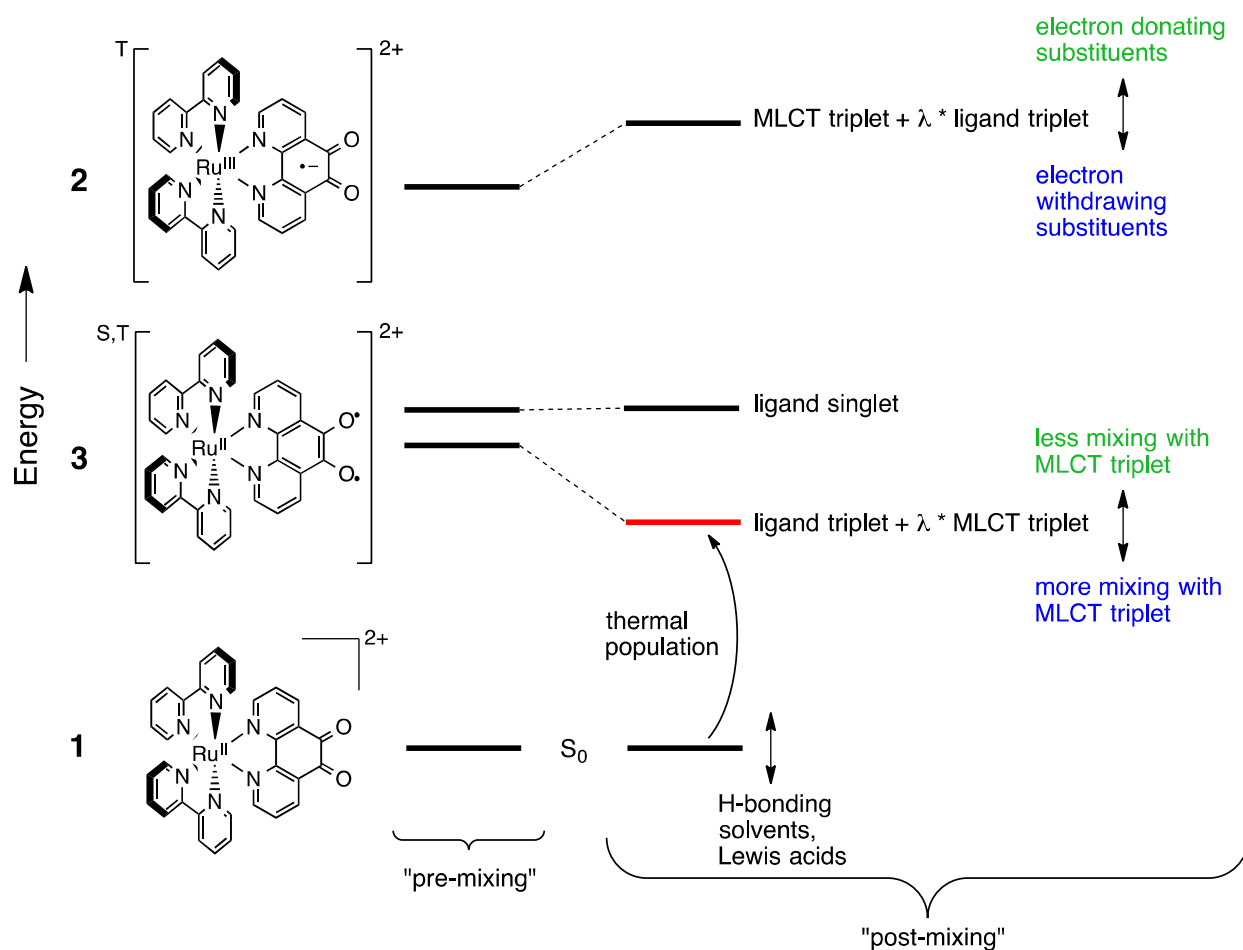


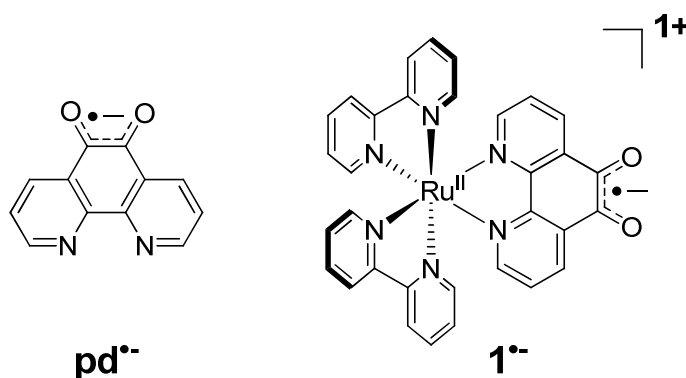
**Figure 9.** A coarse energy level diagram describing substituent and solvent effects responsible for the paramagnetic behavior observed in **1**. The ligand singlet state, while formally a resonance structure of the ground state of **1**, is largely unaffected by configuration interaction from the MLCT triplet (**2**). The ligand triplet state (**3**) mixes with **2** (the mixing coefficient  $\lambda$  is the same in both new (paramagnetic) states thus created). The lower of these two new states (in red) is populated thermally by the ground state, a process that can become symmetry allowed through admixture of singlet character into the MLCT state. Vertical arrows to the right of each state describe its variation with solvent, substituent, or degree of mixing (based on substituent effects that alter the energy of the "pure" MLCT triplet state (in green and blue text)).

It is instructive at this point to note that there may be substantial spectral overlap of the phendione triplet with the MLCT triplet state, a situation that would strongly support the energy level diagram and variations put forward in Figure 9, and would also help to explain our observed substituent effects. To the best of our knowledge the triplet energy of phendione has

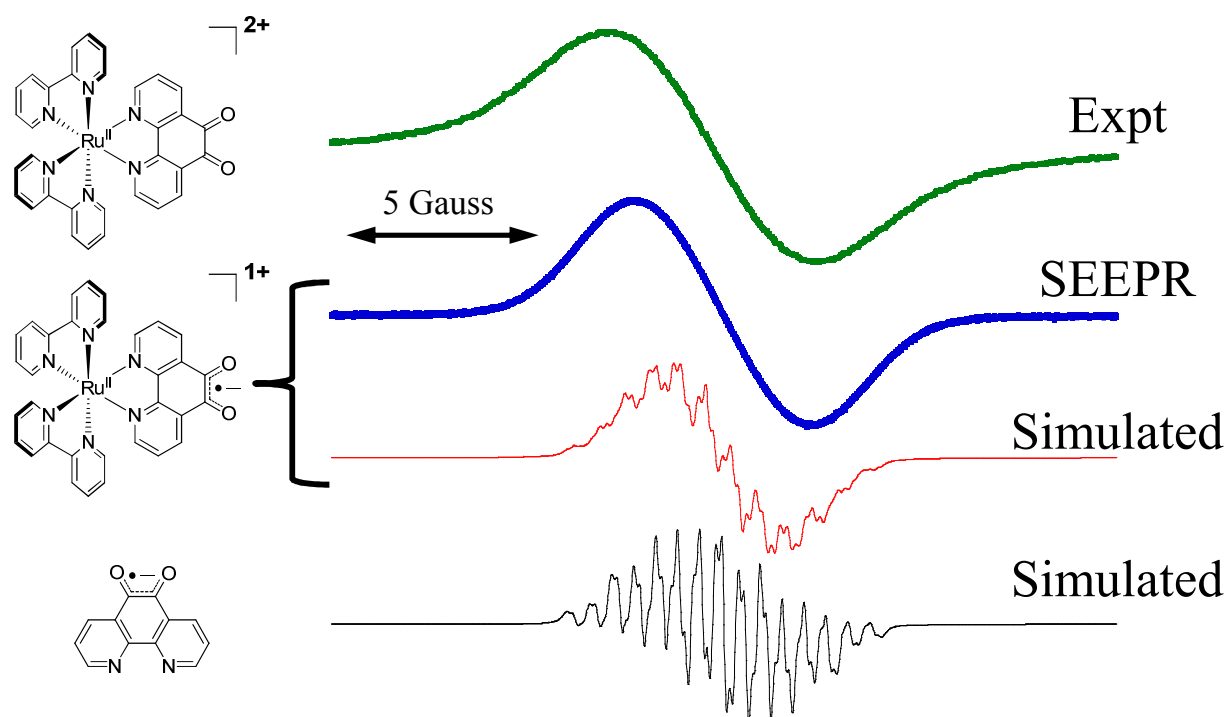
not been measured, but several papers report optical emission from similar complexes,<sup>24-27</sup> the most relevant of which is that from  $[\text{Zn}(\text{phen})_3]^{2+}$ , at about 700 nm.<sup>27</sup> Due to the very low impact of the metal on the ligand's electronic properties, this should be very close to the free ligand emission wavelength and would almost certainly be assigned to the triplet state. This places the triplet at or near the  $^3\text{MLCT}$  state of complex **1**.

Although formally the thermal population of the ground state complex **1** into the mixed ligand/MLCT state is symmetry forbidden, it is well known from the experimental work of McCusker<sup>28</sup> and others,<sup>29-31</sup> and from DFT calculations,<sup>32</sup> that most MLCT states of Ru coordination compounds have substantial singlet character. This admixture of singlet character lifts the forbidden nature of the process.

*G. Control Experiments.* The phendione ligand contains an *ortho*-quinone core, opening the possibility that the paramagnetism observed in samples of **1** is due to the presence of a semiquinone-type radical. The semiquinonate forms of both the free phendione ( $\text{pd}^{\bullet-}$ ) and complex **1** ( $\mathbf{1}^{\bullet-}$ ) are known,<sup>33</sup>



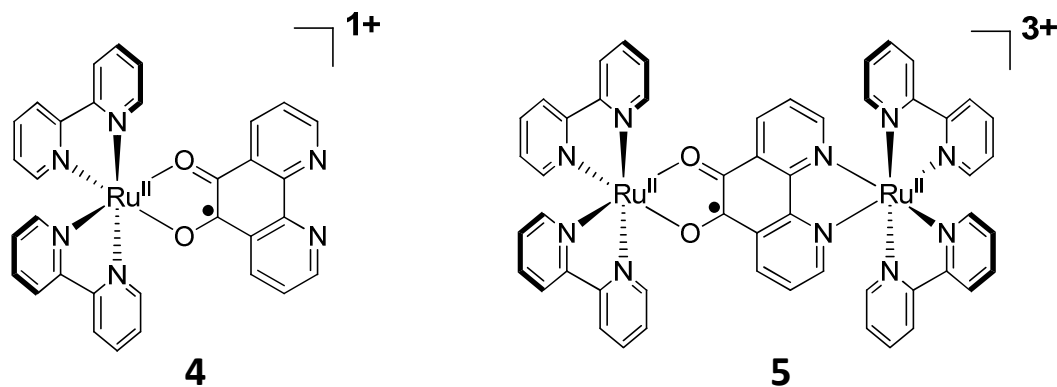
as are several other semiquinonate-containing Ru-phendione complexes.<sup>34,35</sup> We have observed, by direct electrochemical generation, an unresolved EPR spectrum of  $\mathbf{1}^{\bullet-}$ , and a well-resolved EPR spectrum of  $\text{pd}^{\bullet-}$  has been reported.<sup>33</sup> Both species present narrower EPR signals, (Figure 10) than that observed for **1**.



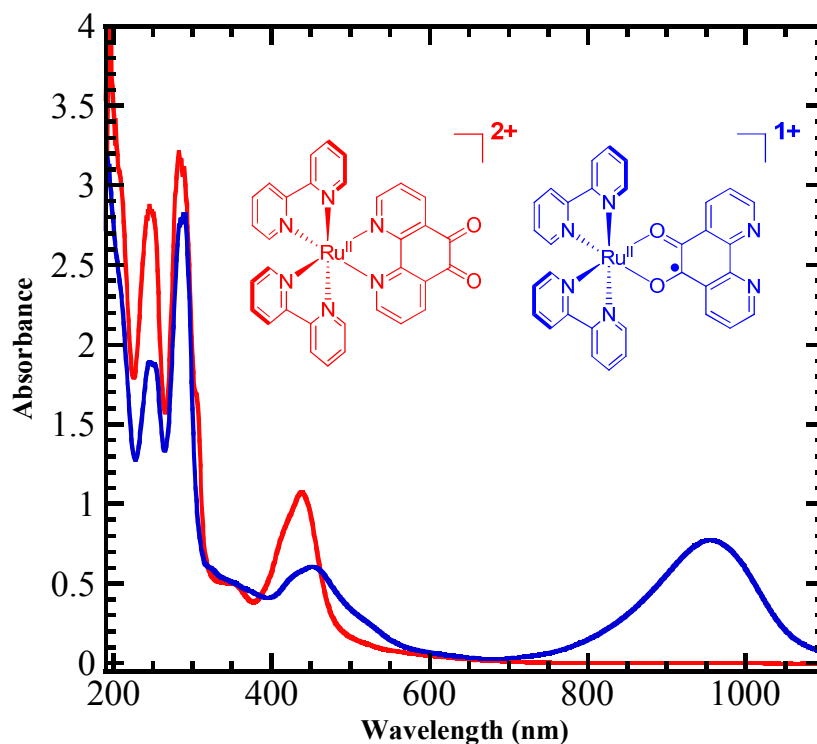
**Figure 10.** Simulated EPR spectra of  $pd^{\bullet-}$  (black) and  $1^{\bullet-}$  (red) using reported hyperfine values,<sup>1</sup> with experimental spectra obtained for **1** (green, from Figure 1) and  $1^{\bullet-}$  (blue, using SEEPR ()) at 5 G modulation included for comparison. Note the narrower spectral width for  $1^{\bullet-}$  (blue) vs. **1** (green).

Figure 10 rules out the participation of either monoradical in this chemistry. Also, if such monoradical species were involved, the EPR signals would increase linearly with concentration rather than decrease as observed (Figure 4). Further confirmation of this result is provided by a lack of contact shifts in the NMR spectrum and in the UV/VIS data (*vide infra*).

The O,O'-bound monomeric and dimeric complexes (**4** and **5**) are alternative reported binding motifs that could also account for the observed paramagnetism if they were present as impurities in these samples. The EPR spectra of these species have been reported.<sup>34,35</sup> Both **4** and **5** are characterized by broad featureless EPR signals with  $g \sim 2.015$  with a total spectral width of ca. 500 G (Supporting Information, Figure S3). We also note that the EPR spectrum of **4** shows a linear increase in signal intensity with concentration, whereas **1** shows a decrease (Figure 4).



Electronic absorption spectra for **1** and **4** were obtained for comparison (Figure 11).



**Figure 11.** Electronic Absorption spectra for **1** and **4**, overlay of **1** in  $\text{CH}_3\text{CN}$  (red) and **4** in  $\text{CH}_3\text{CN}$  (blue).

The absorption spectrum for **4** is dominated by a band at 950 nm, attributed to a  $d(\pi_{\text{Ru}}) \rightarrow \pi^*(\text{sq}_{\text{SOMO}})$  MLCT transition.<sup>34-37</sup> This band is virtually absent in **1**, which is dominated by the typical  $d(\pi_{\text{Ru}}) \rightarrow \pi^*(\text{phendione})$  bpy-localized MLCT band at ca. 435 nm.<sup>38</sup> A key point here is

the absence of any significant absorption for **1** at 950 nm, which indicates the absence of a semiquinone-containing species.

Supporting Information Figure S4 shows that the IR spectrum of **1** is dominated by the C=O absorption at ca.  $1700\text{ cm}^{-1}$ , indicative of the dione moiety.<sup>39,40</sup> The spectrum of **4** lacks this  $1700\text{ cm}^{-1}$  band, and is instead dominated by the typical semiquinone C-O stretch at ca.  $1430\text{ cm}^{-1}$ .<sup>34,35</sup> Based on the comparison of EPR, UV/VIS, and IR spectra of **1** and **4**, it is clear that the O,O'-bound semiquinonate structure **4** cannot be responsible for the observed paramagnetic behavior. Additionally, the  $^1\text{H-NMR}$  spectrum for **4** shows complete broadening of all of the resonances, expected for a radical species with a permanent magnetic moment (data not shown).

### Summary and Outlook

The detailed experimental investigation into the paramagnetic character of **1** in this report strongly supports a contribution from thermally accessible paramagnetic state **3** in the complex  $\text{Ru}(\text{bpy})_2(\text{phendione})^{2+}$ . The  $^1\text{H-NMR}$  results suggest a small paramagnetic contribution to **1** at room temperature. The primary NMR broadening effect is localized to the phendione resonances, with minor shifts in the bpy proton resonances. The EPR experiments correlate with the onset of broadening in the NMR experiments. Both magnetic resonance datasets show strong temperature dependencies, suggesting thermal population of a paramagnetic state. The presence of an O,O'-bound semiquinonate species is ruled out through NMR, EPR, and optical spectroscopies and their temperature, solvent and concentration dependencies. The observed paramagnetic character also appears to be directly related to metal coordination, which is consistent with the reliance on *N*-coordination in phendione hydration chemistry (electron withdrawing character activates the C=O bond for attack). Stabilization of the ground state closed shell singlet state of **1** by

hydrogen bonding of water to the phendione, or coordination of the carbonyls to a Lewis acid ( $\text{Zn}^{2+}$ ), suppresses the effect. These experimental observations suggest that a thermally accessible triplet state is a reasonable source for the observed paramagnetic behavior, and that two phenomena contribute to the mechanism: 1) mixing of the MLCT excited state with the open shell phendione ligand triplet state, lowering its energy toward the ground state of **1**, and 2) lifting of the spin forbidden nature of the thermal population process by admixture of singlet character in the MLCT state itself. To our knowledge, such paramagnetism is a previously unreported phenomenon in both the free ligand and in this binding motif (i.e. N,N'-bound phendione) involving any other metal center.

The presence of a ligand-localized triplet state offers a secondary energy transfer pathway for rapid relaxation of the  $^3\text{MLCT}$  state. This phenomenon may force a reevaluation of the quenching mechanisms observed in a wider class of ruthenium poly(pyridyl) complexes, which may lead to a greater insight into the function of many of these complexes as luminescent sensors and catalysts.<sup>41</sup> For example, the sensitivity of the paramagnetism to substituent effects and temperature suggests the possibility of spin filtering applications,<sup>11</sup> and the pronounced solvent effect may provide new sensing capabilities in non-aqueous environments. A very particular example is that of light switches for DNA sensing applications: the activation or deactivation of a paramagnetic resonance contributor due to H-bonding or hydrophobic effects is certainly a plausible mechanism for such switching.<sup>42</sup>

Further characterization of the  $[\text{Ru}^{\text{II}}(\text{L})_2(\text{phendione})]^{2+}$  series, insight into the origin of this behavior through DFT calculations, and understanding the deeper implications of this phenomenon towards device characteristics when surface bound, are topics currently under investigation.

## Methods

$[\text{Ru}^{\text{II}}(\text{bpy})_2(\text{phendione})](\text{PF}_6)_2$  and  $[\text{Ru}^{\text{II}}(\text{bpy})_2(\text{O},\text{O}'\text{-pd})](\text{PF}_6)$  were prepared according to reported methods.<sup>34,38</sup> All solvents were obtained from Fisher and used as received, unless noted otherwise.

**$\text{Ru}^{\text{II}}(4,4'\text{-dimethylbpy})_2\text{Cl}_2$ .**  $\text{Ru}^{\text{II}}(4,4'\text{-dimethylbpy})_2\text{Cl}_2$  was prepared by the literature procedure developed for  $\text{Ru}^{\text{II}}(\text{bpy})_2\text{Cl}_2$ .<sup>43</sup>

**$[\text{Ru}^{\text{II}}(4,4'\text{-dimethylbpy})_2(\text{pd})](\text{PF}_6)_2$ .**  $[\text{Ru}^{\text{II}}(4,4'\text{-dimethylbpy})_2(\text{pd})](\text{PF}_6)_2$  was prepared by reacting  $\text{Ru}^{\text{II}}(4,4'\text{-dimethylbpy})_2\text{Cl}_2$  (200 mg, 0.37 mmol) with 1.2 equivalents of phendione (93.6 mg, 0.44 mmol) in thoroughly degassed 1:1 water:ethanol at reflux overnight. If the solvent is not degassed the reaction gives multiple products. Yield: 313 mg (87%).

**$[\text{Ru}^{\text{II}}(4,4',5,5'\text{-tetramethylbpy})_2(\text{pd})](\text{PF}_6)_2$ .**  $[\text{Ru}^{\text{II}}(4,4',5,5'\text{-tetramethylbpy})_2(\text{pd})](\text{PF}_6)_2$  was prepared in the same manner as  $[\text{Ru}^{\text{II}}(4,4'\text{-dimethylbpy})_2(\text{pd})](\text{PF}_6)_2$  with similar yield. The ligand 4,4',5,5'-tetramethylbpy was available from previous studies within the lab.

**$[\text{Ru}^{\text{II}}(4,4'\text{-COOEtbpy})_2(\text{pd})](\text{PF}_6)_2$ .**  $[\text{Ru}^{\text{II}}(4,4'\text{-COOEtbpy})_2(\text{pd})](\text{PF}_6)_2$  was prepared in the same manner as  $[\text{Ru}^{\text{II}}(4,4'\text{-dimethylbpy})_2(\text{pd})](\text{PF}_6)_2$  with similar yield. The ligand 4,4'-COOEtbpy was made according to literature procedure.<sup>44</sup>

**Photophysics.** Steady-state and time-resolved emission experiments were performed on an Edinburgh FLSP920 spectrometer in quartz cuvettes. The TCSPC measurements were collected using an EPL-445 laser with sub-100 ps pulse width.

**DFT Calculations.** Theoretical calculations were carried out by using Density Functional Theory (DFT) as implemented in Gaussian09, revision A.02.<sup>45</sup> Becke's three-parameter hybrid functional<sup>46-49</sup> with the LYP correlation functional<sup>50</sup> (B3LYP) was used. For Ru, the LANL2

relativistic effective core potential and associated uncontracted basis set was used, in combination with the 6-31 g\* basis for the ligands (C, N, O, and H). No solvent was included.

**NMR Spectroscopy.**  $^1\text{H}$  NMR spectra were recorded on a Bruker Ultrashield 600 Plus NMR spectrometer at 600.13 MHz and referenced to the residual solvent proton resonance of water ( $\delta$  4.79 ppm) or acetonitrile ( $\delta$  1.94 ppm). Variable temperature  $^1\text{H}$ -NMR spectra were recorded on a Bruker 500 NMR spectrometer at 500.13 MHz over the temperature range 260 – 340 K and referenced to the residual solvent resonance of acetonitrile ( $\delta$  1.94 ppm).

**EPR Spectroscopy.** All EPR spectra were recorded at X-band (9.43 GHz) at room temperature (unless noted otherwise) on a JEOL FA-100 continuous-wave spectrometer. Powder spectra were recorded at room temperature on solid samples in quartz sample tubes. Fluid samples were collected on anhydrous  $\text{CH}_3\text{CN}$  solutions (0.01 mM – 5 mM) in ca. 1.6 mm OD capillary tubes. Dilutions were prepared from a common 5 mM stock; wet samples were prepared by adding DI water. Variable temperature EPR experiments were conducted with a JEOL ES-DVT4 accessory over the temperature range 233 – 343 K on a 1 mM sample in a ca. 1.6 mm OD capillary tube. All samples were degassed prior to running experiments, either by bubbling with  $\text{N}_2$  gas or by freeze-pump-thaw methods.

**Magnetometry.** Magnetic susceptibilities were measured on a Quantum Design MPMS-XL7 SQUID Magnetometer using an applied field of 0.1 T for Curie plots. Microcrystalline samples (ca. 35 mg) were loaded into gelcap/straw sample holders and mounted to the sample rod with Kapton tape. Data from the gelcap samples were corrected for the sample container and molecular diamagnetism using Pascal's constants as a first approximation.

## Acknowledgements

This material is based upon work supported as part of the UNC EFRC: Center for Solar Fuels, an Energy Frontier Research Center funded by the U.S. Department of Energy, Office of Science, Office of Basic Energy Sciences under Award Number DE-SC0001011. M.D.E.F. acknowledges the National Science Foundation for support of EPR instrumentation through grant CHE-1111873. The authors thank Professor David Shultz, Professor James Cahoon, Dr. Natalia Lebedeva and Dr. David Zigler for helpful discussions.

**Supplementary Information:** DFT calculation of spin densities for the lowest ligand triplet state of **1**, NMR concentration data, solution EPR spectra of **5**, and IR data for **1** and **4**.

## References

- 1 S. A. Wolf, *et al.*, *Science*, 2001, **294**, 1488–1495.
- 2 S. D. Bader and S. S. P. Parkin, *Ann. Rev. Cond. Matt. Phys.*, 2010, **1**, 71–88.
- 3 S. Fantacci and F. De Angelis, *Coordin. Chem. Rev.*, 2011, **255**, 2704–2726.
- 4 C. Lescop, E. Belorizky, D. Luneau and P. Rey, *Inorg. Chem.*, 2002, **41**, 3375–3384.
- 5 X. Zhu, H. Tsuji, K. Nakabayashi, S.-i. Ohkoshi and E. Nakamura, *J. Am. Chem. Soc.*, 2011, **133**, 16342–16345.
- 6 Z. Sun, K.-W. Huang and J. Wu, *J. Am. Chem. Soc.*, 2011, **133**, 11896–11899.
- 7 C. Lambert, *Angew. Chem. Intern. Ed.*, 2011, **50**, 1756–1758.
- 8 T. Kubo, *et al.*, *Org. Letters*, 2007, **9**, 81–84.
- 9 W. W. Porter, T. P. Vaid and A. L. Rheingold, *J. Am. Chem. Soc.*, 2005, **127**, 16559–16566.
- 10 Q. Fu, J. Yang and X.-B. Wang, *J. Phys. Chem. A*, 2011, **115**, 3201–3207.
- 11 C. Herrmann, G. C. Solomon and M. A. Ratner, *J. Am. Chem. Soc.*, 2010, **132**, 3682–3684.
- 12 P. Chen, D. E. Root, C. Campochiaro, K. Fujisawa, and E. I. Solomon, *J. Am. Chem. Soc.*, 2003, **125**, 466–474.
- 13 J. L. Tilson, W. C. Ermler and R. J. Fowler, *Chem. Phys. Letters*, 2011, **516**, 131–136.
- 14 M. D. E. Forbes, and S. R. Ruberu, *J. Phys. Chem.*, 1993, **97**, 13223–13233.
- 15 J. H. van Vleck, *The Theory of Electric and Magnetic Susceptibilities*. (Oxford University Press, 1932).
- 16 S. Yamauchi, *et al. J. Phys. Chem. A*, 2003, **107**, 1478–1485.
- 17 P. J. Angiolillo, H. T. Uyeda, T. V. Duncan and M. J. Therien, *J. Phys. Chem. B*, 2004, **108**, 11893–11903.
- 18 "Laboratory Solvents and Other Liquid Reagents," in *CRC Handbook of Chemistry and Physics*, 93rd Edition (Internet Version 2013), W. M. Haynes, ed., CRC Press/Taylor and Francis, Boca Raton, FL.
- 19 S. Singh and C. N. R. Rao, *Can. J. Chem.*, 1966, **44**, 2611–2615.
- 20 Y. Lei, C. Shi and F. C. Anson, *Inorg. Chem.*, 1996, **35**, 3044–3049.
- 21 Y. Lei and F. C. Anson, *J. Am. Chem. Soc.*, 1995, **117**, 9849–9854.
- 22 E. M. Kober, J. V. Caspar, R. S. Lumpkin and T. J. Meyer, *J. Phys. Chem.*, 1986, **90**, 3722–3734.
- 23 T. Fujihara, T. Wada and K. Tanaka, *Dalton Trans.*, 2004, **4**, 645–652.
- 24 D. M. Boghaeia and F. Behzadian-Asla, *J. Coordin. Chem.*, 2007, **60**, 347–353.
- 25 R. D. Gillard and R. E. E. Hill, *Dalton Trans.*, 1974, 1217–1236.
- 26 K. Larsson, and L. Ohrstrom, *Inorg. Chim. Acta*, 2004, **357**, 657–664.
- 27 A. R. Rezvania, A. Saravania and H. Hadadzadehb, *J. Iran. Chem. Soc.*, 2010, **7**, 825–833.
- 28 J. E. Monat, J. H. Rodriguez, and J. K. McCusker, *J. Phys. Chem. A*, 2002, **106**, 7399–7406.
- 29 D. W. Thompson, A. Ito and T. J. Meyer, *Pure Appl. Chem.*, 2013, **85**, 1257–1305.

- 30 E. M. Kober, and T. J. Meyer, *Inorg. Chem.*, 1984, **23**, 3877–3886.
- 31 J. M. Gardner, M. Abrahamsson, B. H. Farnum and G. J. Meyer, *J. Am. Chem. Soc.*, 2009, **131**, 16206–16214.
- 32 C. Daul, E. J. Baerends and P. Vernooijs, *Inorg. Chem.*, 1994, **33**, 3538–3543.
- 33 D. M. Murphy, *et al.*, *Inorg. Chim. Acta*, 2011, **374**, 435–441.
- 34 A. D. Shukla and A. Das, *Polyhedron* 2000, **19**, 2605–2611.
- 35 T. Ghosh, *et al. J. Biol. Inorg. Chem.*, 2005, **10**, 496–508.
- 36 M. Haga, E. S. Dodsworth and A. B. P. Lever, 1986, *Inorg. Chem.* **25**, 447–453.
- 37 A. B. P. Lever, *et al.*, *J. Am. Chem. Soc.* 1988, **110**, 8076–8084.
- 38 S. Bhattacharya and C. G. Pierpont, *Inorg. Chem.*, 1992, **31**, 35–39.
- 39 C. A. Goss and H. D. Abruna, *Inorg. Chem.*, 1985, **24**, 4263–4267.
- 40 D. M. Boghaei and F. B. Asl, *J. Coordin. Chem.*, 2007, **60**, 1629–1635.
- 41 S. A. Poteet, M. B. Majewski, Z. S. Breitbach, C. A. Griffith, S. Singh, D. W. Armstrong, M. O. Wolf and F. M. MacDonnell, *J. Am. Chem. Soc.*, 2013, **135**, 2419–2422.
- 42 A. E. Friedman, J. C. Chambron, J. P. Sauvage, N. J. Turro and J. K. Barton, *J. Am. Chem. Soc.*, 1990, **112**, 4960–4962.
- 43 B. P. Sullivan, D. J. Salmon and T. J. Meyer, *Inorg. Chem.*, 1978, **17**, 3917–3923.
- 44 P. G. Hoertz, *et al.*, *J. Am. Chem. Soc.*, 2006, **128**, 8234–8245.
- 45 Gaussian 09, Revision **D.01**, M. J. Frisch, G. W. Trucks, H. B. Schlegel, G. E. Scuseria, M. A. Robb, J. R. Cheeseman, G. Scalmani, V. Barone, B. Mennucci, G. A. Petersson, H. Nakatsuji, M. Caricato, X. Li, H. P. Hratchian, A. F. Izmaylov, J. Bloino, G. Zheng, J. L. Sonnenberg, M. Hada, M. Ehara, K. Toyota, R. Fukuda, J. Hasegawa, M. Ishida, T. Nakajima, Y. Honda, O. Kitao, H. Nakai, T. Vreven, J. A. Montgomery, Jr., J. E. Peralta, F. Ogliaro, M. Bearpark, J. J. Heyd, E. Brothers, K. N. Kudin, V. N. Staroverov, R. Kobayashi, J. Normand, K. Raghavachari, A. Rendell, J. C. Burant, S. S. Iyengar, J. Tomasi, M. Cossi, N. Rega, J. M. Millam, M. Klene, J. E. Knox, J. B. Cross, V. Bakken, C. Adamo, J. Jaramillo, R. Gomperts, R. E. Stratmann, O. Yazyev, A. J. Austin, R. Cammi, C. Pomelli, J. W. Ochterski, R. L. Martin, K. Morokuma, V. G. Zakrzewski, G. A. Voth, P. Salvador, J. J. Dannenberg, S. Dapprich, A. D. Daniels, Ö. Farkas, J. B. Foresman, J. V. Ortiz, J. Cioslowski, and D. J. Fox, Gaussian, Inc., Wallingford CT, 2009.
- 46 A. D. Becke, *J. Chem. Phys.*, 1993, **98**, 1372–1377.
- 47 A. D. Becke, *J. Chem. Phys.*, 1993, **98**, 5648–5652.
- 48 A. D. Becke, *Phys. Rev. A*, 1988, **38**, 3098–3100.
- 49 P. J. Stephens, F. J. Devlin, C. F. Chabalowski and M. J. Frisch, *J. Phys. Chem.*, 1994, **98**, 11623–11627.
- 50 C. Lee, W. Yang and R. G. Parr, *Phys. Rev. B Condens. Matter*, 1988, **37**, 785–789.